

Universality in the Anticoncentration of Noisy Quantum Circuits at Finite Depths

Arman Sauliere ,¹ Guglielmo Lami ,¹ Corentin Boyer,¹ Jacopo De Nardis ,¹ and Andrea De Luca ¹

¹*Laboratoire de Physique Théorique et Modélisation, CNRS UMR 8089, CY Cergy Paris Université, 95302 Cergy-Pontoise Cedex, France*

We study the anticoncentration properties of quantum circuits in the presence of different sources of noise. In the *weak-noise regime*, we show that different types of noise act in a similar fashion, leading to a universal distribution for the probability of a given bit-string, largely independent of the specific noise channel or circuit architecture. In addition, we can identify three distinct depth-dependent regimes, each signaled by a different scaling of cross-entropy benchmarking (XEB) fidelity over time. In the shallow-depth regime, noise effects are perturbatively small; in the intermediate regime, circuit-induced fluctuations and noise compete on equal footing; and in the deep-depth regime, the output distribution becomes effectively classical, up to corrections that are exponentially small in the noise strength. We provide quantitative predictions for the anticoncentration of generic circuits at finite depth, which we benchmark with numerical simulations giving perfect agreement even for shallow circuits. Our findings are directly applicable to current quantum processors and demonstrate universal behavior beyond random-matrix-theory regimes which are only applicable at large depths.

Introduction. – Quantum machines have transformative potential in many scientific fields, but current and near-term devices remain limited by external noise [1–10]. Although advances reduce noise levels, only fault-tolerant error correction can effectively suppress errors [4, 11, 12]. Meanwhile, the development of methods to characterize noisy quantum circuits and to benchmark their output remains crucial [13–21].

A widely used benchmarking technique is *random circuit sampling* (RCS), in which one samples bit-strings \mathbf{x} from the output density matrix ρ of a random quantum circuit U . By comparing the observed output statistics with those from an ideal (noise-free) classical simulation of the same circuit, one quantifies the hardware global fidelity. This procedure, known as *cross-entropy benchmarking* (XEB), is experimentally accessible and has attracted significant interest [1, 3, 22–24]. Since XEB compares two replicas of the system—one noisy and one ideal—it can be readily analyzed using effective circuit averaging techniques developed for random unitary circuits [25]. However, it captures only partial information about the *anticoncentration* properties of the output distribution in the computational basis [26–39]. The latter are instead fully encoded in the so-called *probability-of-probabilities distribution* (PoP) [1, 40, 41] $P(w)$, i.e. the average distribution of output probabilities $w = D\langle \mathbf{x} | \rho | \mathbf{x} \rangle$ (for convenience rescaled by the Hilbert space dimension D). The moments of the PoP are the celebrated *Inverse Participation Ratios* (IPR), often used to signal localization and non-ergodicity effects.

In the absence of noise, the PoP for Haar-random quantum states—or equivalently for circuits of sufficiently large depth—follows the Porter–Thomas (PT) distribution [42], that for $D \rightarrow \infty$ takes the simple form $P_{\text{PT}}(w) = e^{-w}$. By contrast, classical random bit-string sampling produces $P_{\text{C}}(w) = \delta(w - 1)$, a distribution that also characterizes quantum devices overwhelmed by

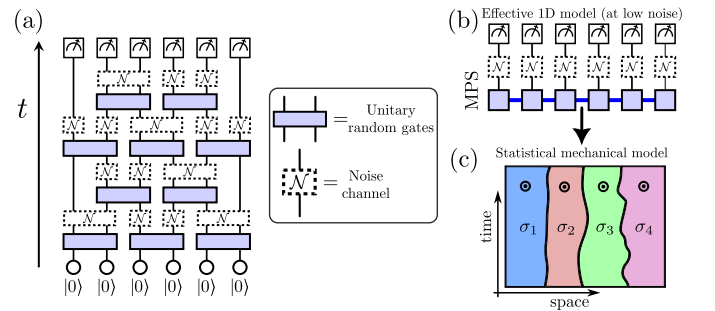


Figure 1. Sketch of the work. (a) We consider the task of random circuit sampling. The circuit is composed by random unitary gates in the usual brickwall geometry, and it is affected by noise represented by a quantum channel \mathcal{N} . We explore noise acting either on single or two-adjacent qubits, all yielding similar conclusions. (b) We identify a specific weak-noise regime where the system becomes effectively one dimensional, and equivalent to a random Matrix Product State (MPS) subject to noise. (c) Replica calculations for the 1D model reveal a statistical model of permutations in an external field, induced by noise, that favors permutations near the identity.

noise. In general, a noisy quantum circuit is expected to interpolate between these two extremes as a function of the noise strength. However, these forms hold strictly in the infinite-depth limit [1, 40, 41]; capturing the quantum–classical crossover at finite depth t requires incorporating finite-depth corrections.

In this letter, we analyze the *combined effects of finite depth and noise* on both the XEB and the full PoP distribution in 1+1 dimensional quantum circuits with open boundary conditions. We focus on the *weak-noise regime* [22, 43], where the error rate per gate ϵ scales as

$$\epsilon \propto \frac{\eta}{N_g}, \quad (1)$$

with $N_g \propto N t$ the total number of gates, and η a positive

parameter that quantifies the number of errors in the circuit. We show the existence of a *scaling regime* in the XEB and PoP distributions under *generic forms of noise*, in the weak-noise regime, characterized by the parameter η and the rescaled inverse circuit depth

$$x = \frac{N}{L(t)}, \quad (2)$$

where $L(t)$ is a characteristic length governing the approach to random-matrix behavior (often dubbed Thouless length) [35, 36, 44–46]. Guided by analytical results, we take this length to behave as $L(t) = L_0 e^{t/\tau}$, with an exponential growth with time t set by two model- and noise-dependent functions, τ and L_0 . Specifically, Eq. (2) refers to a regime of shallow circuits, with $t \sim \tau \log N$. Within this scaling, we identify *three distinct dynamical regimes*, determined by the interplay between x and η , and fully characterize the PoP distribution $P_{x,\eta}(w)$ in each of them, thereby elucidating the quantum-to-classical crossover at finite depth.

We obtain these universal results analytically by means of a description in terms of simple Random Matrix Product States (RMPS) [47–52] subjected to noise, see Fig. 1 and a noisy random unitary circuit – the random phase model (RPM) [36, 44] – in the limit of large local Hilbert space dimension. By extensive numerical simulations, we show that our conclusion is universally applied to generic noisy random circuits with brickwall architectures, which are well-established paradigmatic models of quantum many-body chaotic systems [25, 53–63], together with different forms of experimental noise. Our results provide a unified framework for understanding how noise and finite depth jointly shape the benchmarking metrics of near-term quantum processors.

Setup and Methods – We consider a system of N qudits of local dimension d , with total Hilbert space dimension $D = d^N$. The computational basis is labeled by bit strings $|\mathbf{x}\rangle = |x_1, \dots, x_N\rangle$, where $x_i \in \{0, \dots, d-1\}$. The task of *Random Circuit Sampling* (RCS) is to apply a random quantum circuit U to the initial state $|\mathbf{0}\rangle$, yielding $\rho(U) = U|\mathbf{0}\rangle\langle\mathbf{0}|U^\dagger$, and then to sample bit-strings \mathbf{x} from the *output distribution* $p(\mathbf{x}; \rho(U))$, where we define

$$p(\mathbf{x}; \rho) := \langle \mathbf{x} | \rho | \mathbf{x} \rangle. \quad (3)$$

To fix ideas, we consider a brickwall circuit with alternating layers of two-qudit gates, all independently drawn from the Haar measure $\text{Haar}(d^2)$ (see Fig. 1). In realistic settings, these gates are subject to noise, modeled by a quantum channel of the form

$$\mathcal{N}(\rho) = \sum_{\alpha} K_{\alpha} \rho K_{\alpha}^\dagger, \quad \sum_{\alpha} K_{\alpha}^\dagger K_{\alpha} = \mathbb{1} \quad (4)$$

where the K_{α} are Kraus operators. An example is the depolarizing channel $\mathcal{N}_{\varepsilon}^{\text{dep.}}(\rho) = (1-\varepsilon)\rho + \varepsilon \frac{\mathbb{1}}{q}$, where ε can

be interpreted as the probability of error per gate, and q is the dimension of the Hilbert space on which the noise acts. We consider two scenarios of local noise: single-qudit noise ($q = d$), or two-qudits noise ($q = d^2$). Under noise, the system evolves in a noisy version $\rho_{\mathcal{N}}(U)$ of the final state, and consequently the output distribution becomes $p(\mathbf{x}; \rho_{\mathcal{N}}(U))$. A crucial quantity to measure the success in RCS is the *linear cross-entropy benchmark* (XEB)

$$\text{XEB}(U) = D \sum_{\mathbf{x}} p(\mathbf{x}; \rho_{\mathcal{N}}(U)) p(\mathbf{x}; \rho(U)) - 1, \quad (5)$$

which is the correlation between the ideal and the noisy distributions. For intermediate system sizes, the XEB can be readily estimated experimentally [1] and, for deep circuits ($t \gg \log N$, i.e. $x \rightarrow 0$) serves as a proxy for the fidelity $\mathcal{F} = \text{Tr}[\rho_{\mathcal{N}}(U)\rho(U)]$ between the ideal target state and its noisy counterpart, provided the noise is sufficiently weak [22, 64]. In particular, this holds when the error rate per-layer $\lambda := \varepsilon N$ is below a critical threshold λ_c [22, 24]. Under this condition, both XEB and fidelity decay as $\sim e^{-\lambda t} \sim e^{-\eta}$ (with the scaling in Eq. (1)). When the condition does not hold, the relation between XEB and fidelity generally breaks down. Here, we assume that $\eta = O(1)$, so that XEB and fidelity coincide at infinite depth, but we precisely identify the discrepancies that emerge when $x > 0$. Other key quantities we analyze are the PoP and its moments, represented by the *Inverse Participation Ratios* (IPRs) [41], defined respectively as

$$\begin{aligned} P(w; U) &= D^{-1} \sum_{\mathbf{x}} \delta(w - D p(\mathbf{x}; \rho_{\mathcal{N}}(U))), \\ I_k(U) &= \sum_{\mathbf{x}} p(\mathbf{x}; \rho_{\mathcal{N}}(U))^k \quad \text{with } k \geq 1. \end{aligned} \quad (6)$$

These probe the anticoncentration of the final state in the computational basis. Up to a constant factor, the IPR equals the k -th moment of the PoP: $\mathbb{E}[w^k] = D^{k-1} I_k$. Finally, while the quantities defined above depend explicitly on the specific circuit instance U , one can average them over an ensemble of random circuits, thereby defining $\text{XEB} = \mathbb{E}_U[\text{XEB}(U)]$, $I_k = \mathbb{E}_U[I_k(U)]$, and $P(w) = \mathbb{E}_U[P(w; U)]$. To compute such circuit averages $\mathbb{E}_U[\dots]$, we employ Weingarten calculus [65, 66], which expresses the Haar average of k copies of a unitary gate as a sum over permutation operators $\sigma \in S_k$, where S_k is the symmetric group of order k . Specifically, using the vectorized representation of operators $O \rightarrow |O\rangle\langle O|$ and of their inner product $\text{tr}(O^\dagger Q) = \langle\langle O | Q \rangle\rangle$, the Weingarten formula reads [65, 66]

$$\mathbb{E}_{U \sim \text{Haar}(q)} [(U^* \otimes U)^{\otimes k}] = \sum_{\pi, \sigma \in S_k} \text{Wg}_{\pi, \sigma}(q) |\sigma\rangle\langle\pi|. \quad (7)$$

Here, $\text{Wg}(q)$ denotes the $k! \times k!$ Weingarten matrix, which is the pseudo-inverse of the overlaps matrix $G_{\sigma, \pi}(q) := \langle\langle \sigma | \pi \rangle\rangle_q$ (subscript indicates the Hilbert space dimension).

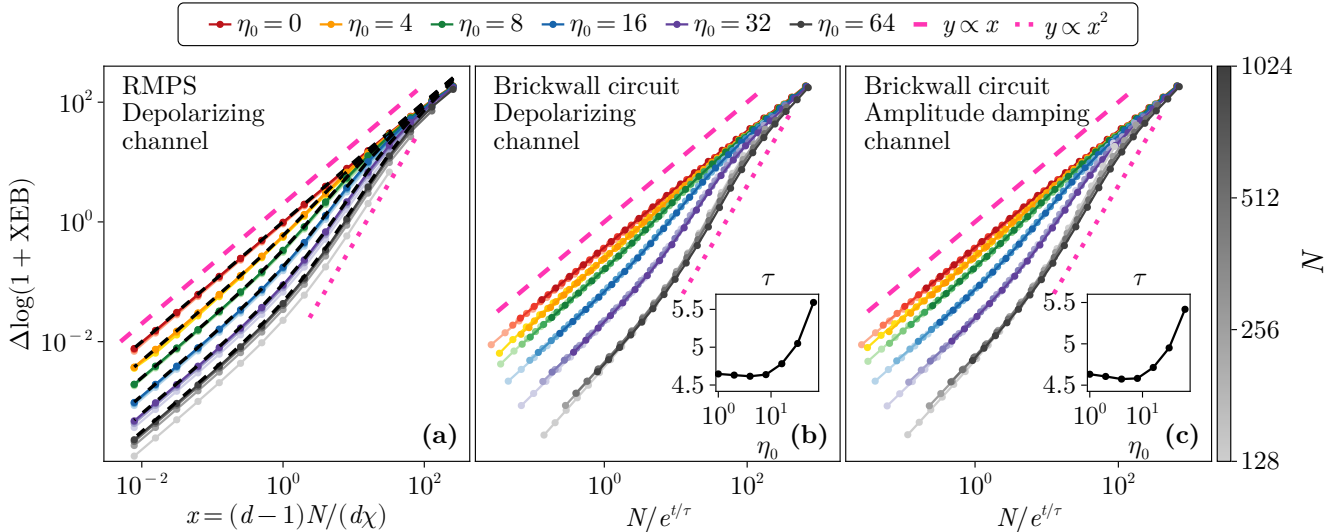


Figure 2. Plot of the XEB both for noisy RMPS (a) and the brickwall circuit (b)-(c). Different noise models are considered: depolarizing channel on physical and bond dimension for the RMPS (a), two-qubit depolarizing noise (b), or single-qubit amplitude damping noise (c). The error rate is fixed as $\epsilon = \eta_0/N$ for RMPS (a), or $\epsilon = \eta_0/(Nt)$ for the circuit (b)-(c). We show that XEB depends only on two parameters x and η_0 . We plot $\Delta \log(1 + \text{XEB}) = \log(1 + \text{XEB}) - \lim_{x \rightarrow 0^+} \log(1 + \text{XEB})$ as a function of x -rescaled circuit's depth. For η_0 large enough, we identify three different scaling regimes. For $x \gg \eta_0$, the scaling is with x and is independent of η_0 , showing that the system is effectively noiseless. Then for $x^2 \sim \eta_0$, the scaling is with x^2 , characteristic of strong noise. For $x < 1$, it goes to its asymptotic value as a linear function of x . In plot (a) we also plot the prediction of Eq. (14) (dashed black line). In the inset we plot the dependence of the Thouless time τ as function of noise rate showing how for weak noise the latter is independent of noise rate as in the RMPS case.

For large q , these matrices can be expanded as

$$G(q) = q^k (\mathbb{1} + q^{-1} A + O(q^{-2})), \quad (8)$$

and $\text{Wg}(q) = q^{-k} (\mathbb{1} - q^{-1} A + O(q^{-2}))$, where the matrix A connects (with unit coefficient) only permutations differing by a single transposition.

Without noise and for global random unitaries $U \sim \text{Haar}(D)$, or equivalently circuits of sufficiently large depth, the PoP follows the well-known *Porter-Thomas* (PT) distribution $P_{\text{PT}}(w) \simeq e^{-w}$, and correspondingly the IPRs are $I_k^{\text{PT}} \simeq k! D^{1-k}$ (both equalities hold for $D \gg 1$). The absence of noise results in a perfect cross-entropy score $\text{XEB}_{\text{PT}} = D I_2 - 1 \simeq 2 - 1 = 1$.

To illustrate instead how noise disrupts these results, let us consider the simple scenario of global depolarizing channel $\rho_{\text{noise}} = \mathcal{N}_{\varepsilon_{\text{glob}}}^{\text{dep.}}(U|\mathbf{0}\rangle\langle\mathbf{0}|U^\dagger)$, with $U \sim \text{Haar}(D)$ as before. In this case, the bitstring distribution $p(\mathbf{x}; \rho_{\text{noise}}(U)) = (1 - \varepsilon_{\text{glob}}) p(\mathbf{x}; \rho(U)) + \frac{\varepsilon_{\text{glob}}}{D}$, and therefore the IPR is $I_k(\varepsilon_{\text{glob}}) = D \sum_{j=0}^k \binom{k}{j} (1 - \varepsilon_{\text{glob}})^{k-j} \left(\frac{\varepsilon_{\text{glob}}}{D}\right)^j \mathbb{E}_U [p(\mathbf{x}; \rho(U))^j]$. By using Eq. (7) to perform the average, this expression can be rewritten as $I_k(\varepsilon_{\text{glob}}) = D^{1-k} \text{Tr}[e^{Q \ln(1 - \varepsilon_{\text{glob}})}]$, with $Q_{\sigma' \sigma} = \delta_{\sigma' \sigma} (k - n_F(\sigma))$ a diagonal $k! \times k!$ matrix that depends on the number of fixed points $n_F(\sigma)$ of the permutation, and plays a central role in our subsequent analysis. The weight $e^{Q \ln(1 - \varepsilon_{\text{glob}})}$ favors permutations with more fixed points, and in the strong

noise limit $\varepsilon_{\text{glob}} \rightarrow 1$, it suppresses all but the identity e (for which $Q_{ee} = 0$). The corresponding PoP is a *shifted Porter-Thomas* (SPT) distribution, given by

$P_{\varepsilon_{\text{glob}}}^{\text{SPT}}(w) = (1 - \varepsilon_{\text{glob}})^{-1} e^{-\frac{w - \varepsilon_{\text{glob}}}{1 - \varepsilon_{\text{glob}}}} \theta(w - \varepsilon_{\text{glob}})$, where $\theta(w)$ is the Heaviside function. The noise parameter $\varepsilon_{\text{glob}}$ is directly linked to the goodness of the cross-entropy benchmarking, as $\text{XEB}_{\text{SPT}} = 1 - \varepsilon_{\text{glob}}$. In the strong noise limit $\varepsilon_{\text{glob}} \rightarrow 1$, the SPT distribution converges to $P_C(w) = \delta(w - 1)$, with corresponding IPRs $I_k^C = D^{1-k}$, reflecting the dominance of the identity permutation e over all others. This delta distribution $P_C(w)$ can thus be interpreted as the classical (i.e. non-quantum) form of the PoP.

Random Matrix Product States model – We now return to consider local quantum circuits where the error rate per gate ϵ is scaled as in Eq. (1). Let us first summarize the results for noiseless unitary evolution ($\eta \rightarrow 0$): it was argued recently Ref. [36], that a universal form of the moments in the scaling limit at fixed x can be derived from an effective one-dimensional model. One way of arguing for this is to formally represent the state $U|\mathbf{0}\rangle$ into an equivalent matrix product state (MPS), with the bond dimension χ growing exponentially in the circuit depth t . Following the arguments of [36, 45], in the scaling limit (s.l.) $N, \chi \rightarrow \infty$ at fixed $x = (d-1)N/(d\chi)$, one

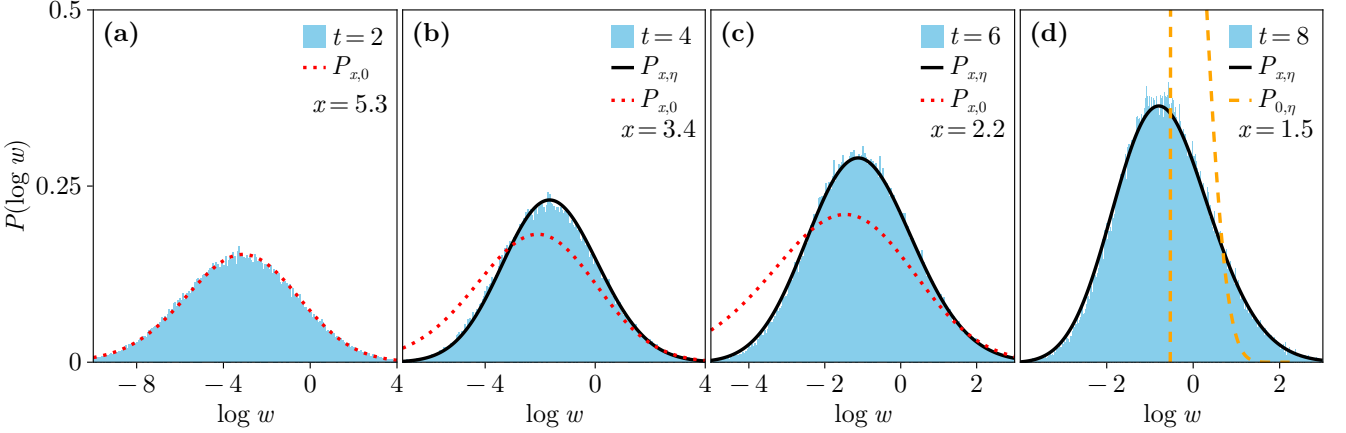


Figure 3. Plot of the PoP distribution for a noisy brickwall circuit featuring two-qubits depolarizing channels. The error rate is defined as $\epsilon = \eta_0/(Nt)$, where $\eta_0 = 2$ and the system size is $N = 32$. Different depths t are explored (see values reported in the plots). At the shortest depth, the distribution is well approximated by the noiseless distribution $P_{x,0}$ (dotted red curve), whereas the latter fails to accurately describe the data at larger depths. In contrast, the theoretically predicted distribution $P_{x,\eta}$ (black line) accurately reproduces the data. The Shifted Porter Thomas (SPT), which corresponds to the distribution for $x = 0$, is also plotted for reference in the last plot.

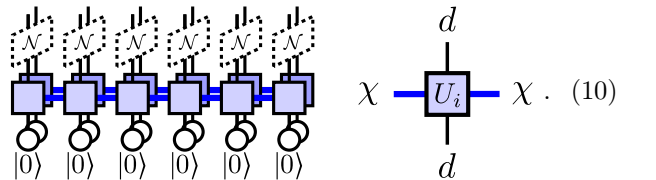
expects that sampling from the resulting MPS is equivalent to sampling from a random matrix product state (RMPS), i.e. one in which the local tensors are random and identically distributed (see below for a precise definition). In this description, the Thouless length in Eq. (2) is identified $L(t) \sim \chi$. Then, the k -replica average expresses the IPRs as the partition function of a 1D statistical mechanical model with local degrees of freedom in the permutation space [34–36]. Such a partition function can be expressed as a product of transfer matrices of size $k! \times k!$, ultimately related to the matrix A introduced above, leading to

$$I_k \stackrel{\text{s.l.}}{=} D^{1-k} (1|e^{xA}|1) = I_k^{\text{PT}} \exp\left(x \frac{k(k-1)}{2}\right). \quad (9)$$

with $|1\rangle = |1 \dots 1\rangle$ a boundary vector of length $k!$ (which is an eigenvector of the matrix A). Finally, one can reconstruct the PoP distribution at any x by recognizing that the moments in Eq. (9) correspond to those of a product of two independent random variables, namely $w = w_{\text{PT}} g$, where w_{PT} is drawn from the Porter–Thomas distribution and g from a log-normal one (such that $\mathbb{E}[g^k] = \exp(xk(k-1)/2)$). These results coincide perfectly with those obtained for the RPM in the limit of large local Hilbert space dimension d [36]. More fundamentally, this reduction to an effectively 1D model is based on the idea that, after coarse-graining, in the space of replicas, the domain walls between distinct permutations extend vertically along the entire depth of the circuit (see Fig. 1(c)): a fact that is ultimately a consequence of the membrane picture [25, 67–69].

We shall show that this approach can be successfully extended to circuits in the presence of noise, obtaining

quantitative predictions for finite-depth circuits. To this end, following the previous argument about reduction to effective 1D models, we model a generic noisy circuit as a noisy RMPS, illustrated by the following tensor network diagram



The unitary matrices U_i ($i \in \{1 \dots, N\}$) have size $d\chi \times d\chi$, where the auxiliary Hilbert space of bond dimension χ is represented by blue links. Since \mathcal{N} acts on the density matrix, both the state and its conjugate are shown (U_i^* with darker shapes). Eq. (10) corresponds to the standard sequential MPS generation starting from qudits in $|0\rangle$ [70], but with single-qubit noise channels \mathcal{N} applied at the end. Equivalently, one can also see Eq. (10) as the action of a random noisy Matrix Product Operator (MPO) applied to the initial state $|0\rangle$. For the moment, we do not need to specify the precise form of the noise channel beyond Eq. (4), but we focus here on the case where it acts only on the physical qudit (Eq. (10)); in the End Matter, we show that our results extend to noise affecting both the physical and bond degrees of freedom. To compute the overlap $w_{\mathbf{x}} = D(\mathbf{x}|\rho_{\mathcal{N}}|\mathbf{x}) = D\langle\langle \mathbf{x}, \mathbf{x}|\rho_{\mathcal{N}}\rangle\rangle$, the open physical legs in Eq. (10) should be contracted with a bit-string \mathbf{x} . It is convenient to express the combined action of noise followed by projection onto x_i as $\langle x_i | \mathcal{N}_i(\rho) | x_i \rangle = \langle\langle \rho_{x_i} | \rho \rangle\rangle_d$ where we define the matrices $\rho_{x_i} := \sum_{\alpha} K_{\alpha}^{\dagger} |x_i\rangle \langle x_i| K_{\alpha}$ from the action of the adjoint noise channel. To compute $I_k = D^{-k} \sum_{\mathbf{x}} \mathbb{E}[w_{\mathbf{x}}^k]$, one

should replicate k times Eq. (10), and using Eq. (7) for each of the matrices U_i . Doing this, one can express the IPR I_k in terms of powers of a transfer matrix ($r = \log_d \chi$, see details in the End matter)

$$I_k = (L|T^{N-r-1}|R), \quad (11)$$

where we set

$$T = \Lambda(d) G(\chi) \text{Wg}(d\chi). \quad (12)$$

The transfer matrix T acts in the space of permutations, thus having size $k! \times k!$. The matrix $\Lambda_{\sigma' \sigma}(d) = \delta_{\sigma' \sigma} \sum_{x_i=0}^{d-1} \langle \langle \rho_{x_i}^{\otimes k} | \sigma \rangle \rangle_d$ is diagonal and encodes the action of the noise channel by giving different weights to permutations. The boundary vectors are $(L) = (1| \text{Wg}(d\chi)$ and $|R) = \Lambda^{r+1}|1)$. For small replica numbers k , Eq. (11) enables the exact evaluation of I_k for arbitrary noise channels, via direct matrix multiplication.

We now proceed to analyze the weak-noise limit. First, we introduce a formal microscopic parameter ε quantifying the *strength* of the channel \mathcal{N} . In particular, for $\varepsilon = 0$, it must reduce to the identity so that we can write $\rho_{x_i} = |x_i\rangle\langle x_i| + \varepsilon \delta \rho_{x_i}$. Now notice that $\langle \langle \rho_{x_i}^{\otimes k} | \sigma \rangle \rangle_d = \prod_{a=1}^k \text{Tr}[(\rho_{x_i})^a]^{n_C(a; \sigma)}$, where $n_C(a; \sigma)$ is the number of cycles of length a in the permutation σ (thus, $n_F(\sigma) = n_C(1; \sigma)$). By expanding this expression in powers of ε , one obtains $\prod_{a=2}^k \text{Tr}[(\rho_{x_i})^a]^{n_C(a; \sigma)} = 1 + \varepsilon \langle x_i | \delta \rho_{x_i} | x_i \rangle Q_{\sigma\sigma} + O(\varepsilon^2)$ and therefore $\Lambda(d) = d(\mathbb{1} - \varepsilon Q + O(\varepsilon^2))$, with $\varepsilon = -\varepsilon d^{-1} \sum_{x_i=0}^{d-1} \langle x_i | \delta \rho_{x_i} | x_i \rangle \propto \varepsilon$ a positive constant (details in End Matter). Note that this result is completely independent of the specific details of the noise (including whether the channel \mathcal{N} is unitary or not). The remaining part of the matrix T can be expanded for large χ using Eq. (8), which yields: $G(\chi) \text{Wg}(d\chi) = 1 + \chi^{-1} \frac{d-1}{d} A + O(\chi^{-2})$.

We are now in the position of discussing the scaling limit. First, consistently with the noiseless case discussed above and Eq. (2), we keep $x = \frac{N}{\chi} \frac{d-1}{d}$ fixed for $N, \chi \rightarrow \infty$. Secondly, we scale the noise strength to zero with system size keeping and $\eta = \varepsilon N$ fixed. Then, Eq. (11) reduces to

$$I_k \stackrel{s.l.}{=} I_k(x, \eta) := D^{1-k} (1| e^{x A - \eta Q} |1). \quad (13)$$

Note that in our modeling using RMPS, a single noise channel per site is present regardless of bond dimension χ . For this reason, $N_g \propto N$ and the parameter η (equivalent as mentioned to the number of errors in the circuit) is scaled exclusively with the spatial dimension. In a quantum circuit extended in time, the number of errors is naturally also proportional to the depth t and $N_g \sim Nt$.

The form (13) for IPRs is one of the main results of this letter. Consistently, it reduces to the noiseless case (9) when $\eta = 0$. As in that case, it effectively describes the partition function of a 1d gas of domain walls with fugacity x in the space of permutations. The parameter η , associated with noise, effectively plays the role of a

magnetic field favoring permutations close to identity. Its universality is based on the fact that in the scaling regime we consider the domain walls are effectively diluted and the particular details of their interactions become negligible; thus, in practice, only two parameters x, η encode for all the microscopic interactions and specific form of the noise.

To the moments (13), it is associated the PoP $P_{x, \eta}(w)$. In the noiseless case ($\eta = 0$), Eq. (13) reduces to Eq. (9) and $P_{x, 0}(w)$ is a log-normal convolved with PT. Moreover, for infinite circuit depth ($x = 0$), one recovers the moments of the SPT distribution (see previous section). Thus, Eq. (13) interpolates between these two regimes, capturing the combined effects of noise and finite depth through the scaling parameters η and x . For small k , Eq. (13) provides an efficient way to compute the scaling form of the IPRs for arbitrary x, η . In particular, in the same framework and scaling limit, we can derive a closed form for the XEB, as it is closely related to I_2 . Technically, the discrepancy between XEB and I_2 lies in the fact that in Eq. (5) only one of the two replicas contains noise, thus leading to XEB $\stackrel{s.l.}{=} DI_2(x, \eta/2) - 1$, and explicitly

$$\text{XEB} \stackrel{s.l.}{=} 2e^{-\eta/2} \left[\cosh(\theta(x, \eta)) + \frac{x \sinh(\theta(x, \eta))}{\theta(x, \eta)} \right] - 1, \quad (14)$$

where $\theta(x, \eta) = \sqrt{x^2 + (\eta/2)^2}$. In the infinite-depth limit one finds $\lim_{x \rightarrow 0^+} \text{XEB} = e^{-\eta}$ which is exactly the value of the fidelity in a noisy RMPS. For practical reasons, we define the deviation from this value in log-scale as $\Delta \log(1 + \text{XEB}) := \log(1 + \text{XEB}) - \lim_{x \rightarrow 0^+} \log(1 + \text{XEB})$.

However, in contrast to the $\eta = 0$ case, an analytic calculation for arbitrary k of the moments from which to reconstruct the explicit form of the distribution is technically complex. Nonetheless, the behavior of the IPRs in different regimes of x can be extracted perturbatively as we show below. Additionally, we provide an effective numerical procedure to extract the PoP.

Dynamical regimes. – For fixed noise η , Eq. (13) and (14) reveal three distinct dynamical regimes traversed changing the circuit depth, and hence x . *Short-depth* $x \gg \eta$. A simple inspection of Eq. (14) shows that $\Delta \log(1 + \text{XEB}) \propto x$ in this regime. Instead, Eq. (13) can be analyzed using perturbation theory in the small parameter η/x , expanding around the noiseless limit $\eta = 0$ (Eq. (9)). At first order, we find $I_k \approx I_k^{\text{PT}} \exp(x \frac{k(k-1)}{2} - \eta(k-1) + O(\eta^2/x))$. The fact that $I_{k \rightarrow 0} \neq D$ (as it trivially should) indicates that the first-order expansion at small η/x cannot be continued analytically at $k < 1$. Nevertheless, it allows us to extract the PoP tails at $w \gg 1$ as a convolution of the PT with a (unnormalized) lognormal. *Large-depth*. To simplify the analysis, we assume that η is large enough that we can focus in practice only on the groundstate of Q , per-

turbed by the matrix A (this amounts to discard term of $O(e^{-2\eta})$). Two relevant types of corrections emerge in Eq. (13): First, from perturbative theory at second order, we get $x^2/(2\eta) \sum_{\sigma} A_{e,\sigma}^2 = x^2 k(k-1)/(4\eta)$. In the domain wall gas interpretation, this can be interpreted as a kink-antikink localized excitation (two identical transpositions) anywhere in the bulk. Second, the boundary state $|1\rangle$ contains every permutation. In particular, transpositions can survive localized at the (left or right) boundary before jumping to identity at the cost of a DW, i.e., $O(x)$. Putting these two contributions together we arrive at $I_k = I_k^C \exp\left(\frac{x^2 k(k-1)}{\eta} \frac{1}{4}\right) \left(1 + \frac{x k(k-1)}{\eta} \frac{1}{2} + O(x^2/\eta^2)\right)$ (see End Matter for details). The first term of this expression again indicates a log-normal PoP (the convolution with the delta distribution $P_C(w)$ is irrelevant). This expression also determines two distinct regimes by increasing the depth of the circuit (decreasing x). When $1 \ll x = \sqrt{\eta} \ll \eta$, the exponential factor dominates giving rise to $\log \mathbb{E}[w^k] \propto x^2/\eta$ behavior. In contrast, at larger depths for which $x \ll 1$, $\log \mathbb{E}[w^k] \propto x/\eta$. This behavior is explicitly confirmed by the analytical expression of the XEB (14).

The existence of these dynamic regimes is a direct consequence of the universal form (13). Fig. 2 presents numerical results for both noisy RMPS and brickwall circuits confirming this analysis. For the latter, we consider two types of noise: a two-qubit depolarizing channel and single-qubit amplitude damping channel. We compute XEB by contracting the tensor network obtained by replicating the system and averaging the unitary gates, which lives in a $k!$ -dimensional space ($k = 2$ for the XEB). While for RMPS the exact form of $x = (N/\chi)(d-1)/d$ is founded before, for the circuit we take $x \propto N/e^{t/\tau}$ and fit the parameter τ . We plot $\Delta \log(1 + \text{XEB})$ as a function of x (RMPS), or $N/e^{t/\tau}$ (circuit). For the circuit, we observe that plotting as a function of this variable yields good collapse of the curves corresponding to different system sizes N . Most importantly, in all three cases, we clearly observe the predicted three regimes $O(x)$, $O(x^2)$ and $O(x)$.

Universal PoP distribution. – The full PoP distribution $P_{x,\eta}(w)$, determined by the moments Eq. (13), is a universal distribution, provided x and η are two model-dependent fitting parameters in generic cases, while for RMPS their explicit form in terms of χ , N and ϵN is known. To show this, in Fig. 3 we compare the distribution arising from our formula Eq. (13) (black lines) with the empirical distribution obtained by computing the overlaps w of random bit-strings with the final state in a random brickwall circuit with two-qubit depolarizing noise (blue histogram) on each gate. The numerical data are obtained from tensor network simulations [71–74] with fixed N and error rate $\epsilon = \eta_0/(Nt)$ on each two-site gate, while we explore different values of depth t .

Extracting the exact value of x and η (which clearly can differ from η_0) is nontrivial due to the absence of analytical expressions for them in the brickwall circuit. Notable, we can compute the XEB (as it can be also done in an experimental setting) and extract η by extrapolating its value at large depth (ideally $x = 0$). Afterwards, we obtain x by setting Eq. (14) equal to the numerical XEB data. These parameters are then used to find the analytical distribution $P_{x,\eta}(w)$ with moments (13). However, the latter remains inaccessible in a closed mathematical form for generic x and η . Using that for sufficiently large $\eta \gg x$, the distribution approaches a log-normal, namely a Gaussian in the variable $\log w$, allows for a systematic expansion. Specifically, we employ the Gram-Charlier A series [75, 76], which approximate a probability distribution in terms of its cumulants. The latter are computed numerically from Eq. (13) for $k \in \{1, 2, 3, 4, 5, 6\}$. In Fig. 3, the empirical distribution and our analytical prediction shows excellent agreement, with small deviations only due the finite size N of the simulation. Dotted red line represents the noiseless distribution $P_{x,0}(w)$ (log-normal convolved with PT), which closely match the empirical distribution for short time t . At late time instead the distribution approaches a Shifted Porter Thomas, i.e. $P_{0,\eta}(w)$ (dashed orange line).

Conclusions – In this work we have investigated the universal properties of anticoncentration in generic, chaotic quantum many-body systems subject to noise. Whereas the influence of noise on infinite-depth circuits, characterized by the Porter–Thomas distribution of overlaps, has been previously studied, here we have focused on the interplay between finite circuit depth and noise, a question of central relevance for near-term quantum devices. We derived a universal form of the distribution of bit-strings probabilities (PoP distribution), as a function of two dimensionless parameters x and η determined by circuit depth, system size, and noise strength. As we have shown, these parameters can be extracted in an experimental setting by measuring the quantity linear cross entropy XEB across different circuit depths. Remarkably, the universal PoP distribution provides an excellent fit to data even from very shallow circuits.

Our analysis is based on an exact mapping to a one-dimensional model of noisy random matrix product states (RMPS). Beyond serving as a tractable theoretical toy model, noisy RMPS are themselves experimentally accessible on current quantum platforms [77–81], whereas random MPO can also be used to benchmark of quantum experiments [82]. Thus, our results not only furnish clear predictions for state-of-the-art quantum machines but also clarify the persistence of genuine quantum effects in the presence of realistic noise.

Acknowledgments – We acknowledge discussions with Xhek Turkeshi and for collaborations on related top-

ics. J.D.N. and G.L. are funded by the ERC Starting Grant 101042293 (HEPIQ) and the ANR-22-CPJ1-0021-01. ADL acknowledges support by the ANR JCJC grant ANR-21-CE47-0003 (TamEnt).

[1] F. Arute, K. Arya, R. Babbush, D. Bacon, J. C. Bardin, R. Barends, R. Biswas, S. Boixo, F. G. Brandao, D. A. Buell, *et al.*, **Nature** **574**, 505–510 (2019).

[2] S. Boixo, S. V. Isakov, V. N. Smelyanskiy, R. Babbush, N. Ding, Z. Jiang, M. J. Bremner, J. M. Martinis, and H. Neven, **Nature Phys.** **14**, 595–600 (2018).

[3] A. Morvan, B. Villalonga, and X. e. a. Mi, **Nature** **634**, 328–333 (2024).

[4] L. Daguerre, R. Blume-Kohout, N. C. Brown, D. Hayes, and I. H. Kim, Experimental demonstration of high-fidelity logical magic states from code switching (2025), [arXiv:2506.14169](https://arxiv.org/abs/2506.14169).

[5] M. Liu, R. Shaydulin, P. Niroula, M. DeCross, S.-H. Hung, W. Y. Kon, E. Cervero-Martín, K. Chakraborty, O. Amer, S. Aaronson, A. Acharya, Y. Alexeev, K. J. Berg, S. Chakrabarti, F. J. Curchod, J. M. Dreiling, N. Erickson, C. Foltz, M. Foss-Feig, D. Hayes, T. S. Humble, N. Kumar, J. Larson, D. Lykov, M. Mills, S. A. Moses, B. Neyenhuis, S. Eloul, P. Siegfried, J. Walker, C. Lim, and M. Pistoia, **Nature** **640**, 343–348 (2025).

[6] Z. Yin, I. Agresti, G. de Felice, D. Brown, A. Toumi, C. Pentangelo, S. Piacentini, A. Crespi, F. Ceccarelli, R. Osellame, B. Coecke, and P. Walther, **Nature Photonics** **10**.1038/s41566-025-01682-5 (2025).

[7] R. Haghshenas, E. Chertkov, M. Mills, W. Kadow, S.-H. Lin, Y.-H. Chen, C. Cade, I. Niesen, T. Begušić, M. S. Rudolph, C. Cirstoiu, K. Hemery, C. M. Keever, M. Lubasch, E. Granet, C. H. Baldwin, J. P. Bartolotta, M. Bohn, J. Cline, M. DeCross, J. M. Dreiling, *et al.*, Digital quantum magnetism at the frontier of classical simulations (2025), [arXiv:2503.20870](https://arxiv.org/abs/2503.20870).

[8] L. Shirizly, G. Misguich, and H. Landa, **Phys. Rev. Lett.** **132**, 010601 (2024).

[9] M. C. Smith, A. D. Leu, K. Miyanishi, M. F. Gely, and D. M. Lucas, **Phys. Rev. Lett.** **134**, 230601 (2025).

[10] B. Rost, L. Del Re, N. Earnest, A. F. Kemper, B. Jones, and J. K. Freericks, **npj Quantum Information** **11**, 10.1038/s41534-025-00964-8 (2025).

[11] D. Aasen, M. Aghaei, Z. Alam, M. Andrzejczuk, A. Antipov, M. Astafev, L. Avilovas, A. Barzegar, B. Bauer, J. Becker, J. M. Bello-Rivas, U. Bhaskar, A. Bocharov, S. Boddapati, D. Bohn, *et al.*, **Roadmap to fault tolerant quantum computation using topological qubit arrays** (2025), [arXiv:2502.12252](https://arxiv.org/abs/2502.12252) [quant-ph].

[12] T. Peham, L. Schmid, L. Berent, M. Müller, and R. Wille, **PRX Quantum** **6**, 020330 (2025).

[13] J. C. Napp, R. L. La Placa, A. M. Dalzell, F. G. S. L. Brandão, and A. W. Harrow, **Phys. Rev. X** **12**, 021021 (2022).

[14] J. Chen, F. Zhang, C. Huang, M. Newman, and Y. Shi, arXiv preprint [arXiv:1805.01450](https://arxiv.org/abs/1805.01450) (2018).

[15] I. L. Markov, A. Fatima, S. V. Isakov, and S. Boixo, arXiv preprint [arXiv:1807.10749](https://arxiv.org/abs/1807.10749) (2018).

[16] C. Huang, F. Zhang, M. Newman, J. Cai, X. Gao, Z. Tian, J. Wu, H. Xu, H. Yu, B. Yuan, M. Szegedy, Y. Shi, and J. Chen, **Classical simulation of quantum supremacy circuits** (2020), [arXiv:2005.06787](https://arxiv.org/abs/2005.06787) [quant-ph].

[17] S. Aaronson and L. Chen, Complexity-theoretic foundations of quantum supremacy experiments (2016), [arXiv:1612.05903](https://arxiv.org/abs/1612.05903) [quant-ph].

[18] V. Pednault, J. A. Gunnels, G. Nannicini, L. Horesh, and R. Wisnieff, Leveraging secondary storage to simulate deep 54-qubit sycamore circuits (2019).

[19] J. Gray and S. Kourtis, **Quantum** **5**, 410 (2021).

[20] S. Bravyi, D. E. Browne, P. Calpin, E. Campbell, D. Gosset, and M. Howard, arXiv preprint [arXiv:1808.00128](https://arxiv.org/abs/1808.00128) (2018).

[21] T. Vincent, L. J. O’Riordan, M. Andrenkov, J. Brown, N. Killoran, H. Qi, and I. Dhand, arXiv preprint [arXiv:2107.09793](https://arxiv.org/abs/2107.09793) (2021).

[22] X. Gao, M. Kalinowski, C.-N. Chou, M. D. Lukin, B. Barak, and S. Choi, **PRX Quantum** **5**, 10.1103/prxquantum.5.010334 (2024).

[23] B. Ware, A. Deshpande, D. Hangleiter, P. Niroula, B. Feferman, A. V. Gorshkov, and M. J. Gullans, **A sharp phase transition in linear cross-entropy benchmarking** (2023), [arXiv:2305.04954](https://arxiv.org/abs/2305.04954) [quant-ph].

[24] S. Liu, M.-R. Li, S.-X. Zhang, S.-K. Jian, and H. Yao, **Physical Review B** **110**, 10.1103/physrevb.110.064323 (2024).

[25] M. P. Fisher, V. Khemani, A. Nahum, and S. Vijay, **Annual Review of Condensed Matter Physics** **14**, 335–379 (2023).

[26] A. W. Harrow and R. A. Low, **Communications in Mathematical Physics** **291**, 257 (2009).

[27] F. G. S. L. Brandão, A. W. Harrow, and M. Horodecki, **Communications in Mathematical Physics** **346**, 397 (2016).

[28] D. Hangleiter, J. Bermejo-Vega, M. Schwarz, and J. Eisert, **Quantum** **2**, 65 (2018).

[29] A. M. Dalzell, N. Hunter-Jones, and F. G. S. L. Brandão, **PRX Quantum** **3**, 010333 (2022).

[30] D. J. Luitz, N. Laflorencie, and F. Alet, **J. Stat. Mech.: Theor. Exp.** **2014**, P08007 (2014).

[31] D. J. Luitz, F. Alet, and N. Laflorencie, **Phys. Rev. Lett.** **112**, 057203 (2014).

[32] E. Tirrito, X. Turkeshi, and P. Sierant, **Anticoncentration and magic spreading under ergodic quantum dynamics** (2024), [arXiv:2412.10229](https://arxiv.org/abs/2412.10229) [quant-ph].

[33] N. Macé, F. Alet, and N. Laflorencie, **Phys. Rev. Lett.** **123**, 180601 (2019).

[34] A. Sauliere, B. Magni, G. Lami, X. Turkeshi, and J. De Nardis, **Universality in the anticoncentration of chaotic quantum circuits** (2025), [arXiv:2503.00119](https://arxiv.org/abs/2503.00119) [quant-ph].

[35] G. Lami, J. De Nardis, and X. Turkeshi, **Physical Review Letters** **134**, 10.1103/physrevlett.134.010401 (2025).

[36] A. Christopoulos, A. Chan, and A. De Luca, **Universal distributions of overlaps from generic dynamics in quantum many-body systems** (2025), [arXiv:2404.10057](https://arxiv.org/abs/2404.10057) [cond-mat.stat-mech].

[37] B. Magni, A. Christopoulos, A. De Luca, and X. Turkeshi, Anticoncentration in clifford circuits and beyond: From random tensor networks to pseudo-magic states (2025), [arXiv:2502.20455](https://arxiv.org/abs/2502.20455).

[38] P. W. Claeys and G. De Tomasi, **Phys. Rev. Lett.** **134**, 050405 (2025).

[39] D. K. Mark, F. Surace, A. Elben, A. L. Shaw, J. Choi, G. Refael, M. Endres, and S. Choi, **Phys. Rev. X** **14**, 041051 (2024).

[40] A. Kaufman, J. Corona, Z. Ozzello, B. Senseman, M. Asaduzzaman, and Y. Meurice, Improved entanglement entropy estimates from filtered bitstring probabilities (2024), [arXiv:2411.07092](https://arxiv.org/abs/2411.07092).

[41] A. L. Shaw, D. K. Mark, J. Choi, R. Finkelstein, P. Scholl, S. Choi, and M. Endres, *Universal fluctuations and noise learning from hilbert-space ergodicity* (2024), [arXiv:2403.11971](https://arxiv.org/abs/2403.11971) [quant-ph].

[42] C. E. Porter and R. G. Thomas, *Phys. Rev.* **104**, 483 (1956).

[43] A. M. Dalzell, N. Hunter-Jones, and F. G. S. L. Brandão, *Communications in Mathematical Physics* **405**, 10.1007/s00220-024-04958-z (2024).

[44] A. Chan, A. De Luca, and J. T. Chalker, *Phys. Rev. Lett.* **121**, 060601 (2018).

[45] S. Shivam, A. De Luca, D. A. Huse, and A. Chan, *Physical Review Letters* **130**, 10.1103/physrevlett.130.140403 (2023).

[46] A. Chan, S. Shivam, D. A. Huse, and A. De Luca, *Nature Communications* **13**, 10.1038/s41467-022-34318-1 (2022).

[47] S. Garnerone, T. R. de Oliveira, and P. Zanardi, *Phys. Rev. A* **81**, 032336 (2010).

[48] S. Garnerone, T. R. de Oliveira, S. Haas, and P. Zanardi, *Phys. Rev. A* **82**, 052312 (2010).

[49] D. Haag, F. Baccari, and G. Styliaris, *PRX Quantum* **4**, 030330 (2023).

[50] C. Lancien and D. Pérez-García, *Annales Henri Poincaré* **23**, 141–222 (2021).

[51] G. Lami, T. Haug, and J. De Nardis, *PRX Quantum* **6**, 010345 (2025).

[52] Z. Cheng, X. Feng, and M. Ippoliti, *Phys. Rev. Lett.* **135**, 020403 (2025).

[53] A. Nahum, S. Vijay, and J. Haah, *Physical Review X* **8**, 021014 (2018).

[54] L. Logarić, S. Dooley, S. Pappalardi, and J. Goold, *Phys. Rev. Lett.* **132**, 010401 (2024).

[55] A. Chan, A. De Luca, and J. Chalker, *Physical Review X* **8**, 041019 (2018).

[56] A. Chan, A. De Luca, and J. Chalker, *Physical Review Letters* **121**, 060601 (2018).

[57] A. Chan, A. De Luca, and J. Chalker, *Physical Review Letters* **122**, 220601 (2019).

[58] B. Bertini, P. Kos, and T. Prosen, *Physical Review Letters* **123**, 210601 (2019).

[59] L. Piroli, B. Bertini, J. Cirac, and T. Prosen, *Physical Review B* **101**, 094304 (2020).

[60] D. E. Parker, H. Cao, B. Swingle, and X.-L. Qi, *Physical Review X* **9**, 041017 (2019).

[61] J. S. Cotler, N. Hunter-Jones, J. Liu, B. Yoshida, and X.-L. Qi, *Journal of High Energy Physics* **2017**, 48 (2017).

[62] S. Gopalakrishnan, R. Vasseur, and A. Potter, *Physical Review B* **101**, 060303 (2020).

[63] N. Hunter-Jones, J. Cotler, J. Liu, B. Yoshida, and X.-L. Qi, *Journal of High Energy Physics* **2018**, 121 (2018).

[64] A. M. Dalzell, N. Hunter-Jones, and F. G. S. L. Brandão, *Random quantum circuits transform local noise into global white noise* (2021), [arXiv:2111.14907](https://arxiv.org/abs/2111.14907) [quant-ph].

[65] G. Köstenberger, *Weingarten Calculus* (2021), [arXiv:2101.00921](https://arxiv.org/abs/2101.00921) [math.PR].

[66] B. Collins, S. Matsumoto, and J. Novak, *Notices of the American Mathematical Society* **69**, 1 (2022).

[67] T. Zhou and A. Nahum, *Phys. Rev. B* **99**, 174205 (2019).

[68] T. Zhou and A. Nahum, *Phys. Rev. X* **10**, 031066 (2020).

[69] A. De Luca, C. Liu, A. Nahum, and T. Zhou, Universality classes for purification in nonunitary quantum processes (2023), [arXiv:2312.17744](https://arxiv.org/abs/2312.17744) [cond-mat.stat-mech].

[70] C. Schon, K. Hammerer, M. M. Wolf, J. I. Cirac, and E. Solano, *Phys. Rev. A* **75**, 032311 (2007).

[71] G. Vidal, *Physical Review Letters* **93**, 040502 (2004).

[72] M. Zwolak and G. Vidal, *Physical Review Letters* **93**, 207205 (2004).

[73] F. Verstraete, J. J. García-Ripoll, and I. Cirac, *Physical Review Letters* **93**, 207204 (2004).

[74] M. Fishman, S. R. White, and E. M. Stoudenmire, *SciPost Phys. Codebases* , 4 (2022).

[75] J. P. Gram, *Matematisk-fysiske Meddelelser fra Det Kongelige Danske Videnskabernes Selskab* **6**, 1 (1883).

[76] C. V. L. Charlier, *Acta Mathematica* **29**, 309 (1905).

[77] L. Piroli, G. Styliaris, and J. I. Cirac, *Phys. Rev. Lett.* **127**, 220503 (2021).

[78] D. Malz, G. Styliaris, Z.-Y. Wei, and J. I. Cirac, *Phys. Rev. Lett.* **132**, 040404 (2024).

[79] K. C. Smith, A. Khan, B. K. Clark, S. M. Girvin, and T.-C. Wei, [arXiv:2404.16083](https://arxiv.org/abs/2404.16083).

[80] D. T. Stephen and O. Hart, [arXiv:2404.16360](https://arxiv.org/abs/2404.16360).

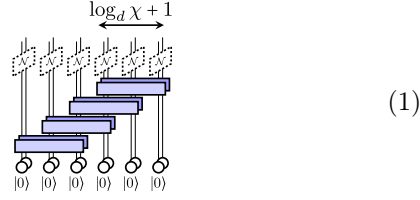
[81] Y. Zhang, S. Gopalakrishnan, and G. Styliaris, [arXiv:2405.09615](https://arxiv.org/abs/2405.09615).

[82] M. Votto, M. Ljubotina, C. Lancien, J. I. Cirac, P. Zoller, M. Serbyn, L. Piroli, and B. Vermersch, Learning mixed quantum states in large-scale experiments (2025), [arXiv:2507.12550](https://arxiv.org/abs/2507.12550).

End Matter

DERIVATION OF THE RMPS TRANSFER MATRIX AND WEAK NOISE EXPANSION OF THE TRANSFER MATRIX Λ

Here, we provide a full derivation of the replica tensor network for the noisy RMPS model (namely of Eq. (11)). The staircase circuit which generates the RMPS is



This representation is essentially equivalent to Eq. (10), but with the unitaries reshaped as gates and the boundary conditions properly accounted for. Unitaries U_i , of size $d\chi \times d\chi$, act on $r + 1$ qudits, with $r = \log_d \chi$ ($r = 2$ in Eq. (1)). To compute the overlap $w_{\mathbf{x}} = D\langle \mathbf{x}, \mathbf{x} | \rho_{\mathcal{N}} \rangle$ for a fixed bit-string \mathbf{x} , one must contract the open physical legs in Eq. (1) with the state $\langle \mathbf{x}, \mathbf{x} |$; that is,

$$w_{\mathbf{x}} = D\langle \mathbf{x} | \rho_{\mathcal{N}} \rangle = D\langle \rho_{x_1}, \dots, \rho_{x_N} | \prod_{i=1}^{N-r} (U_i^* \otimes U_i) (|0, 0\rangle)^{\otimes N} | \rangle, \quad (2)$$

where $\rho_{x_i} = \sum_{\alpha} K_{\alpha}^{\dagger} |x_i\rangle \langle x_i| K_{\alpha}$ capture the combined action of noise $\mathcal{N}_i(\rho) = \sum_{\alpha} K_{\alpha} \rho K_{\alpha}^{\dagger}$ followed by projection onto x_i . To compute the IPR $I_k = D^{-k} \sum_{\mathbf{x}} \mathbb{E}[w_{\mathbf{x}}^k]$, one must replicate the network k times, sum over all \mathbf{x} and perform the average over the U_i . This results in

$$I_k = \mathbb{E} \left[\left(\langle \rho_{x_1}, \dots, \rho_{x_N} | \prod_{i=1}^{N-r} (U_i^* \otimes U_i) (|0, 0\rangle)^{\otimes N} \right)^{\otimes k} \right]. \quad (3)$$

Now we employ the Weingarten formula

$$\begin{aligned} \mathbb{E}_{U \sim \text{Haar}(d\chi)} [(U^* \otimes U)^{\otimes k}] &= \\ &= \sum_{\pi, \sigma \in S_k} \text{Wg}_{\pi, \sigma}(d\chi) |\sigma\rangle_d |\sigma\rangle_{\chi} \langle \pi|_{\chi} \langle \pi|_d, \end{aligned} \quad (4)$$

where we explicitly used the factorization $|\sigma\rangle_{d\chi} = |\sigma\rangle_d |\sigma\rangle_{\chi}$. This equation has to be applied for all matrices U_i . In the d -dimensional spaces, the permutations are either contracted with $|0, 0\rangle$, resulting in an irrelevant factor $\langle \pi | (|0, 0\rangle)^{\otimes k} = 1$, or with the noise boundary vectors $|\rho_{x_i}\rangle$. In this case, the permutations acquire a weight $\langle \rho_{x_i} | \sigma \rangle_d$. We can incorporate the sum over x_i in this weight, thus obtaining $\sum_{x_i=0}^{d-1} \langle \rho_{x_i} | \sigma \rangle_d$. For convenience, we define the $k! \times k!$ matrix $\Lambda_{\sigma' \sigma}(d) = \delta_{\sigma' \sigma} \sum_{x_i=0}^{d-1} \langle \rho_{x_i} | \sigma \rangle_d$, which encodes the weights on the diagonal. The last gate of the staircase U_{N-r} has all the $r + 1$ output legs contracted with the noise, thus resulting in a weight

$R_{\sigma} = (\sum_{x_i=0}^{d-1} \langle \rho_{x_i} | \sigma \rangle_d)^{r+1}$, which defines the right boundary vector $|R\rangle = \Lambda^{r+1} |1 \dots 1\rangle$ of length $k!$. The left boundary vector, instead, is obtained by contracting the permutation obtained from U_1 with the state $|0, 0\rangle$, also incorporating the associated Weingarten coefficients. This results in $\langle L | = (1 | \text{Wg}(d\chi))$. In the χ -dimensional spaces, permutations resulting from consecutive matrices U_i , U_{i+1} are contracted together, giving rise to the overlaps matrix $G_{\sigma, \pi}(\chi) = \langle \sigma | \pi \rangle_{\chi}$. Putting together all these terms one finally obtain Eq. (11), with the transfer matrix defined as in Eq. (12).

Now let us see in details how the Λ matrix expands for weak noise. As in the main text, we write $\rho_{x_i} = |x_i\rangle \langle x_i| + \varepsilon \delta \rho_{x_i}$, and the expansion goes as follows

$$\begin{aligned} \langle \rho_{x_i} | \sigma \rangle_d &= \text{Tr}[\rho_{x_i}]^{\text{nF}(\sigma)} \prod_{a=2}^k \text{Tr}[(\rho_{x_i})^a]^{\text{nC}(a; \sigma)} = \\ &= (1 + \varepsilon \text{Tr}[\delta \rho_{x_i}])^{\text{nF}(\sigma)} \prod_{a=2}^k (1 + \varepsilon a \langle x_i | \delta \rho_{x_i} | x_i \rangle + O(\varepsilon^2))^{\text{nC}(a; \sigma)} = \\ &= 1 + \varepsilon \left(\text{Tr}[\delta \rho_{x_i}] \text{nF}(\sigma) + \langle x_i | \delta \rho_{x_i} | x_i \rangle \left(\sum_{a=2}^k a \text{nC}(a; \sigma) \right) \right) \\ &\quad + O(\varepsilon^2). \end{aligned}$$

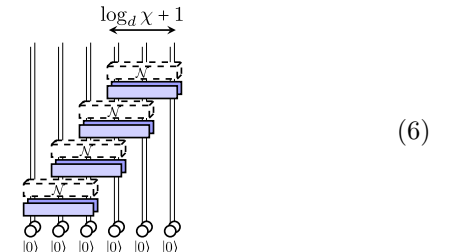
Now notice that $\sum_{a=2}^k a \text{nC}(a; \sigma) = \sum_{a=1}^k a \text{nC}(a; \sigma) - \text{nF}(\sigma) = k - \text{nF}(\sigma) = Q_{\sigma\sigma}$. Furthermore, summing the above expression over x_i leads to a simplification, since $\sum_{x_i=0}^{d-1} \delta \rho_{x_i} = \varepsilon^{-1} (\sum_{x_i=0}^{d-1} \rho_{x_i} - \sum_{x_i=0}^{d-1} |x_i\rangle \langle x_i|) = 0$. This yields

$$\begin{aligned} \Lambda_{\sigma\sigma} &= \sum_{x_i=0}^{d-1} \langle \rho_{x_i} | \sigma \rangle_d = 1 + \varepsilon Q_{\sigma\sigma} \sum_{x_i=0}^{d-1} \langle x_i | \delta \rho_{x_i} | x_i \rangle + O(\varepsilon^2) = \\ &= 1 - \epsilon Q_{\sigma\sigma} + O(\varepsilon^2), \end{aligned} \quad (5)$$

where by definition $\epsilon = -\varepsilon \sum_{x_i=0}^{d-1} \langle x_i | \delta \rho_{x_i} | x_i \rangle$. Notice that this parameter is positive since $\varepsilon \sum_{x_i=0}^{d-1} \langle x_i | \delta \rho_{x_i} | x_i \rangle = \sum_{x_i=0}^{d-1} (\langle x_i | \rho_{x_i} | x_i \rangle - 1)$, and $0 \leq \langle x_i | \rho_{x_i} | x_i \rangle \leq 1$ because $\rho_{x_i} \geq 0$ and $\text{Tr}[\rho_{x_i}] \leq 1$.

NOISY LADDER CIRCUIT

Here, we consider a different model of noisy RMPS, where the noise acts on both the physical qudits and the bond dimension. As a result, the corresponding staircase circuit representation, analogous to Eq. (1), is given by



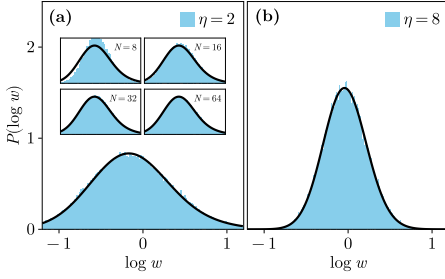


Figure 1. PoP of RMPS under a depolarizing channel on both physical and bond dimension for $N = 128$, $\chi = 128$ ($x = 0.5$), and $2 \leq \eta \leq 8$. The distribution of $\log w$ can be approximated as a Gram-Charlier A series (black line) where only the first two terms of the expansion have been considered and the cumulants of the distribution have been fitted from I_k computed from Eq. (13) for $k \in \{1, \dots, 6\}$. Inset of panel (a) shows the approach to the universal prediction by increasing N .

In the vectorized formalism, the combined action of the unitary gates followed by the noise is $\mathcal{N}_\epsilon^{\text{dep.}}((U \otimes U^*)|\rho\rangle\langle\rho|)$, where ρ is a certain trial density matrix. For simplicity, we assume a specific form of noise, namely the depolarizing channel $\mathcal{N}_\epsilon^{\text{dep.}}(\rho) = (1 - \epsilon)\rho + \epsilon \frac{1}{q}$, where $q = d\chi = d^{r+1}$ is the Hilbert space dimension on which $\mathcal{N}_\epsilon^{\text{dep.}}$ acts on. In this case, we have

$$\mathcal{N}_\epsilon^{\text{dep.}}((U \otimes U^*)|\rho\rangle\langle\rho|) = (1 - \epsilon)(U \otimes U^*)|\rho\rangle\langle\rho| + \frac{\epsilon}{q}|e\rangle\langle e|\rho\rangle\langle\rho|, \quad (7)$$

where e is the identity permutation (which contracted with ρ gives $\langle e|\rho\rangle\langle\rho| = \text{Tr}[\rho]$). Since we want to perform replica calculations, i.e. averaging k -replicas of Eq. (6), the crucial quantity of interest is for us

$$\begin{aligned} \mathbb{E}_U[(\mathcal{N}((U \otimes U^*)|\rho\rangle\langle\rho|))^{\otimes k}] &= \\ &= \mathbb{E}_U\left[\left((1 - \epsilon)U \otimes U^* + \frac{\epsilon}{q}|e\rangle\langle e|\right)^{\otimes k}\right]|\rho\rangle\langle\rho|^{\otimes k}, \end{aligned} \quad (8)$$

where, by linearity, the trial density matrix is taken outside the average. We now assume the following form

$$\begin{aligned} \mathbb{E}_U\left[\left((1 - \epsilon)U \otimes U^* + \frac{\epsilon}{q}|e\rangle\langle e|\right)^{\otimes k}\right] &= \\ &= \sum_{\pi, \sigma \in S_k} \tilde{Wg}_{\pi, \sigma}(q, \epsilon) |\sigma\rangle\langle\pi|, \end{aligned} \quad (9)$$

which is justified in analogy with Eq. (7), and where $\tilde{Wg}_{\pi, \sigma}(q, \epsilon)$ denote *noisy Weingarten coefficients* that remain to be determined.

To find these coefficients, we fix σ and π , and observe that each common fixed point of the two permutations can be obtained in the expansion of the left-hand side of Eq. (9) from a term $|e\rangle\langle e|$ appearing in a specific position, while the remaining part of the two permutations should be obtained from the average of $U \otimes U^*$. Taking these observations into account, we arrive at

$$\tilde{Wg}_{\pi, \sigma}(q, \epsilon) = \sum_{i=0}^{\text{nf}(\pi, \sigma)} \binom{\text{nf}(\pi, \sigma)}{i} \frac{\epsilon^i}{q^i} (1 - \epsilon)^{k-i} Wg_{\tilde{\pi}(i), \tilde{\sigma}(i)}^{(k-i)}(q), \quad (10)$$

where $\text{nf}(\pi, \sigma)$ denotes the number of common fixed points between π and σ , and $\tilde{\pi}(i)$, $\tilde{\sigma}(i)$ denote the permutations obtained from π , σ , respectively, by removing i of these common fixed points (which ones is unimportant, because Wg depends only the cycle structure).

We can now compute the IPR I_k and expressing it, in analogy with Eq. (11), as

$$I_k = D(L|T^{N-r-1}|R) \quad (11)$$

where now the transfer matrix is $T = G(\chi) \tilde{Wg}(d\chi)$, $(L) = (1|\tilde{Wg}(d\chi)$ and $|R) = |1)$.

As in the main text, we focus on the scaling limit $N, \chi \rightarrow \infty$, $\epsilon \rightarrow 0$ with $x \propto N/\chi$ and $\eta = \epsilon N$ fixed. In this regime, it is sufficient to expand the transfer matrix to first order in $1/\chi$ and ϵ , which is equivalent to retaining only the leading-order terms in $1/N$. Noting that, in Eq. (10), only the terms with $i = 0, 1$ contribute at this order, we write: $\tilde{Wg}_{\pi, \sigma}(d\chi, \epsilon) = (d\chi)^{-k} \left((1 - \frac{k\eta}{N})(\delta_{\pi, \sigma} - \frac{1}{d\chi} A_{\pi, \sigma}) + \frac{\eta}{N} \text{nf}(\sigma) \delta_{\pi, \sigma} + O(\frac{1}{N^2}) \right)$, which gives $\tilde{Wg}(d\chi) = (d\chi)^{-k} \left(1 - \frac{1}{d\chi} A - \frac{\eta}{N} Q + O(\frac{1}{N^2}) \right)$. Hence, the transfer matrix in Eq. (11) can be written as

$$T = d^{-k} \left(1 + \frac{1}{N} (xA - \eta Q) + O(N^{-2}) \right), \quad (12)$$

which allows to recover Eq. (13) in the scaling limit. In Fig. 1, we present the PoP distribution of noisy RMPS constructed as in Eq. (6) for a specific value of x and various values of η . There is a strong agreement between the experimental distribution and the Gram-Charlier A series. Furthermore, in Fig. 1(a), we illustrate how the data approach the Gram-Charlier expansion as the system size N increases.